

Radial excitations of Q -balls, and their D -term

Manuel Mai¹ and Peter Schweitzer²

¹*Department of Physics Yale University, New Haven, CT 06511-8499, U.S.A.*

²*Department of Physics, University of Connecticut, Storrs, CT 06269, U.S.A.*

(Dated: June 2012)

We study the structure of the energy-momentum tensor of radial excitations of Q -balls in scalar field theories with $U(1)$ symmetry. The obtained numerical results for the $1 \leq N \leq 23$ excitations allow us to study in detail patterns how the solutions behave with N . We show that although the fields $\phi(r)$ and energy-momentum tensor densities exhibit a remarkable degree of complexity, the properties of the solutions scale with N with great regularity. This is to best of our knowledge the first study of the D -term d_1 for excited states, and we demonstrate that it is negative — in agreement with results from literature on the d_1 of ground state particles.

PACS numbers: 11.10.Lm, 11.27.+d

Keywords: energy momentum tensor, Q -ball, soliton, stability, D -term

I. INTRODUCTION

The energy momentum tensor $T_{\mu\nu}$ (EMT) is a central quantity in the field theoretical description of particles. Its matrix elements [1] give the mass [2], the spin [3], and the constant d_1 of a particle [4] to which we shall loosely refer as the D -term. Though not known experimentally, d_1 is a particle property as fundamental as mass, spin, electric charge or magnetic moment. Its physical meaning is that it gives unique insights into the distribution of internal (in hadrons: strong) forces [5].

EMT form factors found little practical applications [6], until it became clear that they can be accessed by means of generalized parton distribution functions [7, 8] in hard exclusive reactions such as deeply virtual Compton scattering [9–12]. Since that the EMT form factors were investigated in theoretical frameworks including chiral perturbation theory, lattice QCD, or effective chiral field theories, see [4, 5] and [13–19].

Remarkably, in all theoretical studies d_1 of pions, nucleons, nuclei was found negative. A possible explanation of this observation provide chiral soliton models [17, 18], which describe the nucleon in the limit of a large number of colors N_c in QCD [20]. In these models the negative sign of d_1 emerges as a natural consequence of the stability of the nucleon [17, 18].

To shed some light on the question whether $d_1 < 0$ is a general and model-independent feature, in Ref. [21] the EMT of Q -balls was studied. These non-topological solitons appear in theories with global symmetries, and it is the appearance of the associated conserved charge(s) which plays a crucial role for their existence [22–24].

Q -balls have numerous applications in astrophysics, cosmology, and particle physics [25–44]. They provide an extremely fruitful framework for the purpose of clarifying the relation d_1 and stability arguments. In [21] an extensive study of the EMT structure of ground state solutions was presented. In all cases $d_1 < 0$ was found, and a rigorous proof was formulated that the D -term of Q -balls must be negative. Moreover, it was shown that stability is a sufficient but not necessary condition for d_1

to be negative, because some ground state solutions describe absolutely stable, others meta-stable or unstable Q -balls, depending on the parameters. The general proof applies to all cases and always $d_1 < 0$ [21].

This work is dedicated to the study of the EMT of radial excitations of Q -balls in scalar field theories with $U(1)$ symmetry. To best of our knowledge, this is the first study of the D -term going beyond the description of a ground state. Radial excitations of Q -balls were studied previously in [36], where the ground state and the first two excited states $N = 1, 2$ were found for a fixed value of the charge Q . In this work, we will work with a fixed value of the angular velocity ω in the $U(1)$ -space, and study the first $1 \leq N \leq 23$ excitations. With $N = 0$ denoting ground states, the family of Q -ball solutions can hence be classified by specifying (Q, N) as done in [36], or by specifying (ω, N) as chosen in this work.

Our numerical results reach high in the spectrum of radial excitations and give fascinating and detailed insights in the properties of excited Q -balls. In particular, we will see that also excited states have a negative d_1 . The present work extends and completes our study of the EMT structure of ground state Q -balls. It is important to remark that we make no effort to describe the full spectrum of Q -balls which would include also vibrational or other excitations [23], and we will not consider quantum corrections [31].

The lay-out of this work is as follows. In Sec. II we will briefly introduce the framework, and review how radial excitations of Q -balls emerge [36]. In Sec. III we will present the solutions for the ground state and radial excitations $1 \leq N \leq 23$ which we were able to find with our numerical method, and discuss the charge density and the EMT densities. In Sec. IV we will discuss global properties like charge, mass, mean square radii, and the D -term and investigate patterns how these properties scale with N . Remarkably, among the studied quantities d_1 varies most strongly with N . Finally, in Sec. V we will focus on the issue of stability and the sign of the D -term. The conclusions will be presented in Sec. VI, and some technical questions addressed in Appendices.

II. Q-BALLS AND RADIAL EXCITATIONS

In this Section we briefly review the theory of Q -balls, and introduce the indispensable formulae on the EMT. We use throughout the notation of [21], and refer to it for more details. We study the relativistic field theory of a complex scalar field $\Phi(x)$ with global $U(1)$ symmetry

$$\mathcal{L} = \frac{1}{2} (\partial_\mu \Phi^*) (\partial^\mu \Phi) - V, \quad (1)$$

where, for suitable potentials V [23], Q -balls emerge as finite energy solutions of the type $\Phi(t, \vec{x}) = \exp(i\omega t) \phi(r)$ with $r = |\vec{x}|$ and $\phi(r)$ satisfying the equation of motion

$$\phi''(r) + \frac{2}{r} \phi'(r) + \omega^2 \phi - V'(\phi) = 0, \quad (2)$$

$$\phi(0) \equiv \phi_0, \quad \phi'(0) = 0, \quad \phi(r) \rightarrow 0 \text{ for } r \rightarrow \infty.$$

We will use the potential $V(\phi) = A\phi^2 - B\phi^4 + C\phi^6$ with $A = 1.1$, $B = 2.0$, $C = 1.0$ [21, 36], and set $\omega^2 = 1.37$ which is among the ideal values for our purposes, see App. A.

To demonstrate the existence of ground (and excited) Q -ball states, one can identify $r \rightarrow t$ and $\phi(r) \rightarrow x(t)$ [23], and interpret (2) as the Newtonian equation for a unit mass particle moving under the influence of the friction $F_{\text{fric}} = -\frac{2}{t} \dot{x}(t)$ in an effective potential $U_{\text{eff}} = \frac{1}{2}\omega^2 x^2 - V$,

$$\ddot{x}(t) = F_{\text{fric}} - \nabla U_{\text{eff}}(x). \quad (3)$$

A ground state solution corresponds to the situation that the particle starts at $t = 0$ from rest at $x_0 \rightarrow \phi_0$, and its motion terminates in the origin $x = 0$ after infinite time.

In this picture radial excitations correspond to the situation when the particle is given more potential energy such that it overshoots the point $x = 0$, moves “up-hill” in the effective potential till it reaches a point of return, and finally comes to rest at the origin. In principle, the starting points can be chosen such that the particle will overshoot the origin 1, 2, 3, \dots , N times, see Fig. 1. This means the corresponding solution $\phi(r)$ has N nodes at finite r , and we refer to it as the N^{th} radial excitation. The ground state correspond to $N = 0$.

This picture helps to anticipate several features of the excitations. As N increases, the particle has to travel longer paths, and do more work against the friction. Thus we have to release it “close” to the maximum of U_{eff} where the effective potential is nearly flat, see Fig. 1. The particle has to “wait” there for a sufficiently long time before “sliding” down the potential, such the time-dependent friction is adequately decreased to allow the particle to complete its trajectory.

Therefore, as N increases, ϕ_0 approaches the position of the maximum of U_{eff} , see App. A, and $\phi(r) \simeq \phi_0$ remains basically constant over increasingly extended plateaus “to wait for the frictional force” to diminish. The small- r behavior which follows from (2) is [21]

$$\phi(r) = \phi_0 - \frac{U'_{\text{eff}}(\phi_0)}{6} r^2 + \frac{U'_{\text{eff}}(\phi_0) U''_{\text{eff}}(\phi_0)}{120} r^4 + \mathcal{O}(r^6). \quad (4)$$

$U_{\text{eff}}(x)$

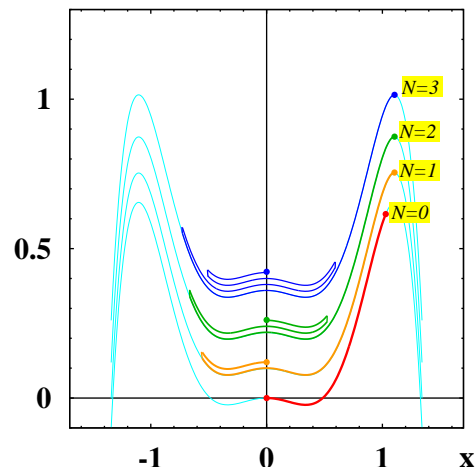


FIG. 1: The effective potential $U_{\text{eff}}(x) = \frac{1}{2}\omega^2 x^2 - V(x)$ as used in this work vs. x (thin line). The particle trajectories are indicated for $N = 0, 1, 2, 3$ (solid lines). For better visibility for $N = (1, 2, 3)$ the potentials are displaced by $(0.1, 0.22, 0.36)$ as compared to $N = 0$, and the particle trajectories are displaced by 0.02 after each turn.

In this Taylor expansion only even powers of r occur, and we checked that the coefficients c_k for $k = 6, 8, 10, 12$ are also proportional to $U'_{\text{eff}}(\phi_0)$ though the expressions become lengthy. This explains why $\phi(r)$ exhibits a plateau. After the plateau we expect $\phi(r)$ to “oscillate” N -times, before it vanishes at asymptotically large r according to [21]

$$\phi(r) \rightarrow \frac{c_\infty}{r} \exp\left(-r\sqrt{\omega_{\text{max}}^2 - \omega^2}\right). \quad (5)$$

With our numerical method described in App. A we were able to find solutions for the first $N = 23$ excited states.

In the following we will discuss the charge density ρ_{ch} , and the EMT densities, namely energy density, $T_{00}(r)$, pressure and shear force distributions, $p(r)$ and $s(r)$, which are given by [21]

$$\rho_{\text{ch}}(r) = \omega \phi(r)^2, \quad (6)$$

$$T_{00}(r) = \frac{1}{2}\omega^2 \phi(r)^2 + \frac{1}{2} \phi'(r)^2 + V(\phi), \quad (7)$$

$$s(r) = \phi'(r)^2, \quad (8)$$

$$p(r) = \frac{1}{2}\omega^2 \phi(r)^2 - \frac{1}{6} \phi'(r)^2 - V(\phi). \quad (9)$$

We also define the conserved charge $Q = \int d^3x \rho_{\text{ch}}(r)$ due to the $U(1)$ -symmetry of the theory (1), the mass $M = \int d^3x T_{00}(r)$, and the constant d_1 which can be expressed equivalently in terms of $s(r)$ and $p(r)$ as follows

$$d_1 = -\frac{1}{3} M \int_0^\infty d^3x r^2 s(r) = \frac{5}{4} M \int_0^\infty d^3x r^2 p(r). \quad (10)$$

The large- r asymptotics (5) ensures that the integrals defining Q , M , d_1 are well-defined.

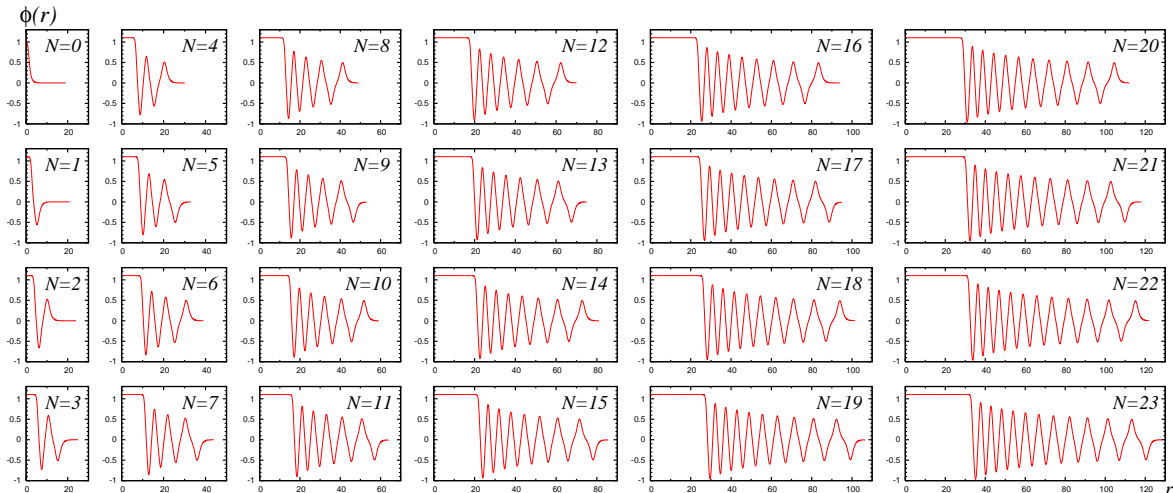


FIG. 2: The fields $\phi(r)$ as functions of r for $0 \leq N \leq 23$.

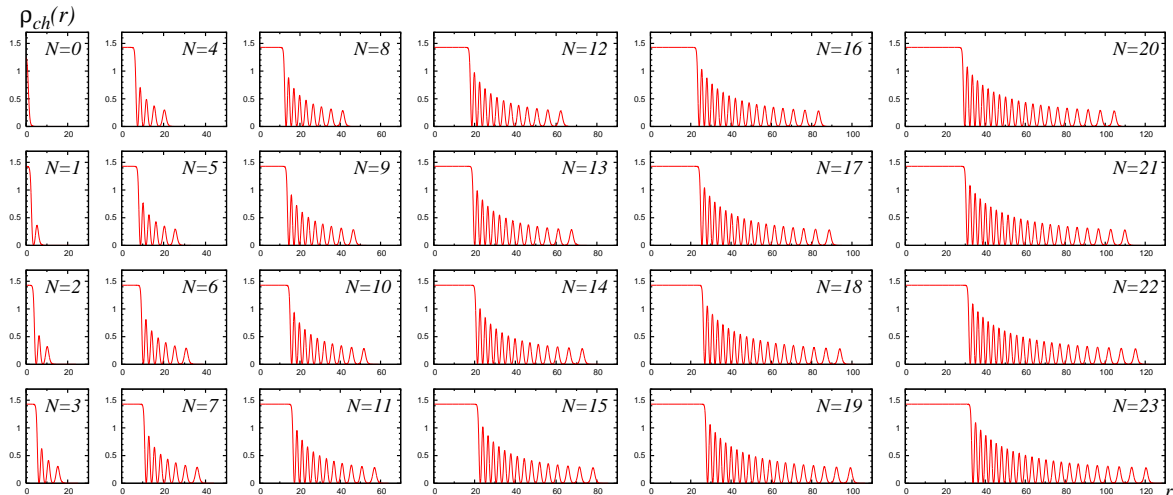


FIG. 3: The charge distributions $\rho_{\text{ch}}(r)$ as functions of r for $0 \leq N \leq 23$.

III. RESULTS FOR THE DENSITIES

Fig 2 shows the results for the radial fields $\phi(r)$, the ground state $N = 0$ and radial excitations $1 \leq N \leq 23$. The results confirm the features we predicted in Sec. II. For $N > 0$ the initial values ϕ_0 are numerically within 10^{-6} close to each other. For $N \gtrsim 2$ the solutions show plateaus with $\phi(r) \simeq \phi_0$, followed by regions of “oscillatory behavior” with N zeros, before the exponential decays set in according to (5). For $N \gtrsim 4$ the sizes of the plateau regions and oscillatory regions are roughly in a constant 1 : 3 ratio.

The N zeros of the solutions $\phi(r)$ imply a strict shell structure for the charge distributions $\rho_{\text{ch}}(r)$ which is shown in Fig. 3. The N^{th} excited state consists of an inner region of nearly constant charge density for $N \gtrsim 4$, followed by an outer region with N shells.

Also the energy densities $T_{00}(r)$ in Fig. 4 exhibit characteristic shell structures. Although they never vanish at finite r , the $T_{00}(r)$ show noticeable minima numerically

very close to the zeros of $\rho_{\text{ch}}(r)$. This can be understood in the particle motion picture as follows. We have $T'_{00}(r) = \frac{\partial}{\partial t} E_{\text{kin}}$ for $r \in \{R_i | \phi(R_i) = 0, 1 \leq i \leq N\}$, i.e. the positions R_i , where the fields and hence also charge distributions vanish, correspond in time to the transits of the particle through the origin, and $T'_{00}(R_i)$ correspond to time-derivatives of the kinetic energies at those times. In the absence of frictional forces E_{kin} would be exactly extremal at the origin. Because of friction the extrema of E_{kin} are somewhat shifted, but those shifts decrease with time (\leftrightarrow distance) because $F_{\text{fric}} \propto \frac{1}{t}$.

For $N \gtrsim 2$ the energy densities show “spikes” at the edge of the inner bulk region. For $N \gtrsim 3$ also the subsequent inner shells exhibit characteristic “double-spike” structures. The reason for that is the contribution of the surface energy [21]. The concepts of surface tension and surface energy are well defined for $\omega \rightarrow \omega_{\text{min}}$ [23], but the associated features are noticeable also away from this limit [21]. If the inner region and the N shells had sharp edges, $s(r)$ would consist of $(2N + 1)$ δ -functions

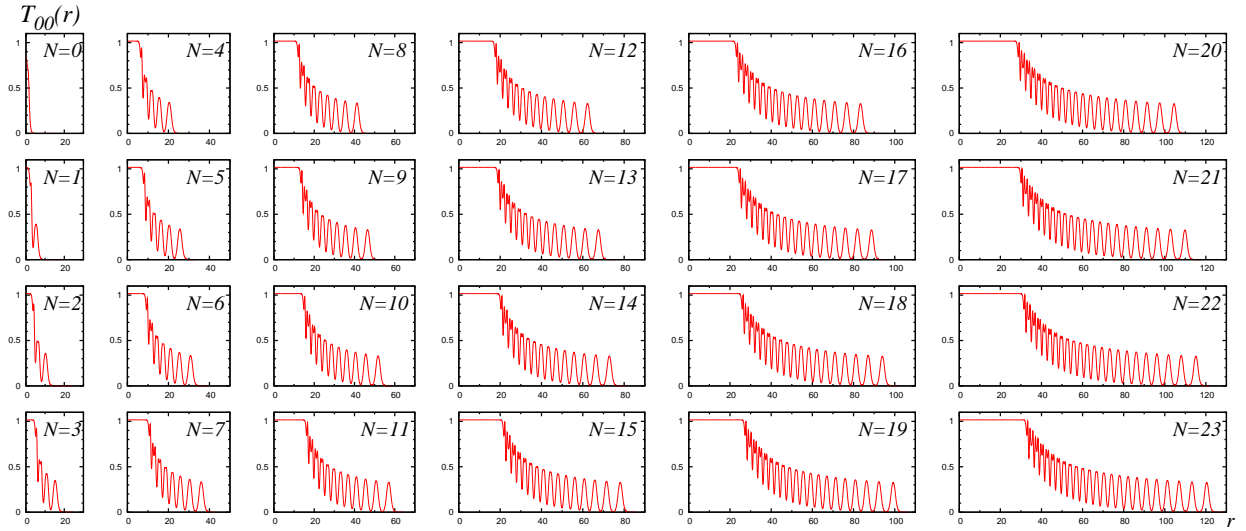


FIG. 4: The energy densities $T_{00}(r)$ as functions of r for $0 \leq N \leq 23$.

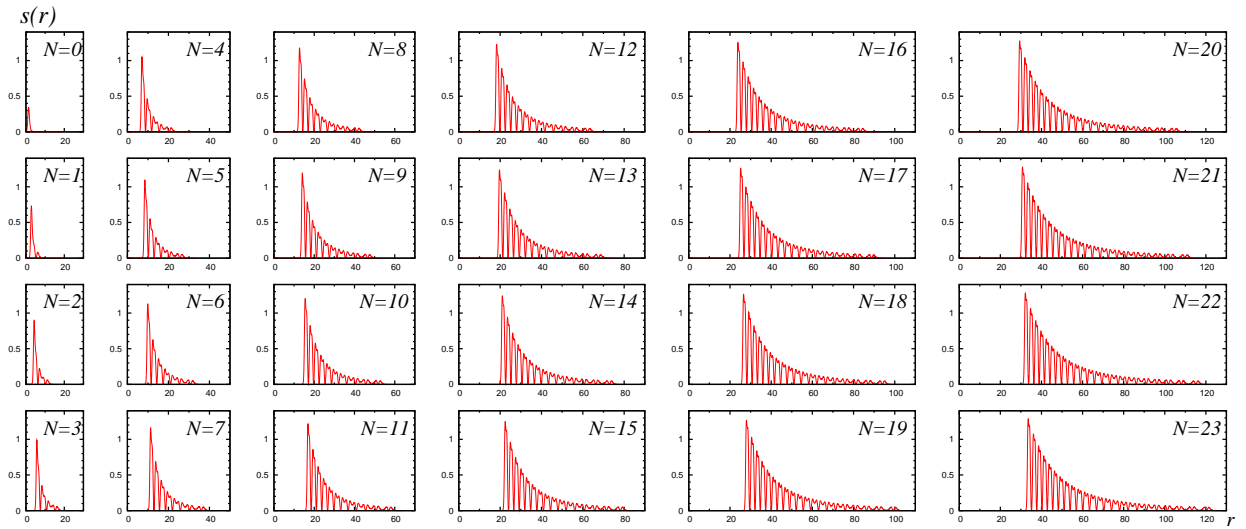


FIG. 5: The shear force distributions $s(r)$ as functions of r for $0 \leq N \leq 23$.

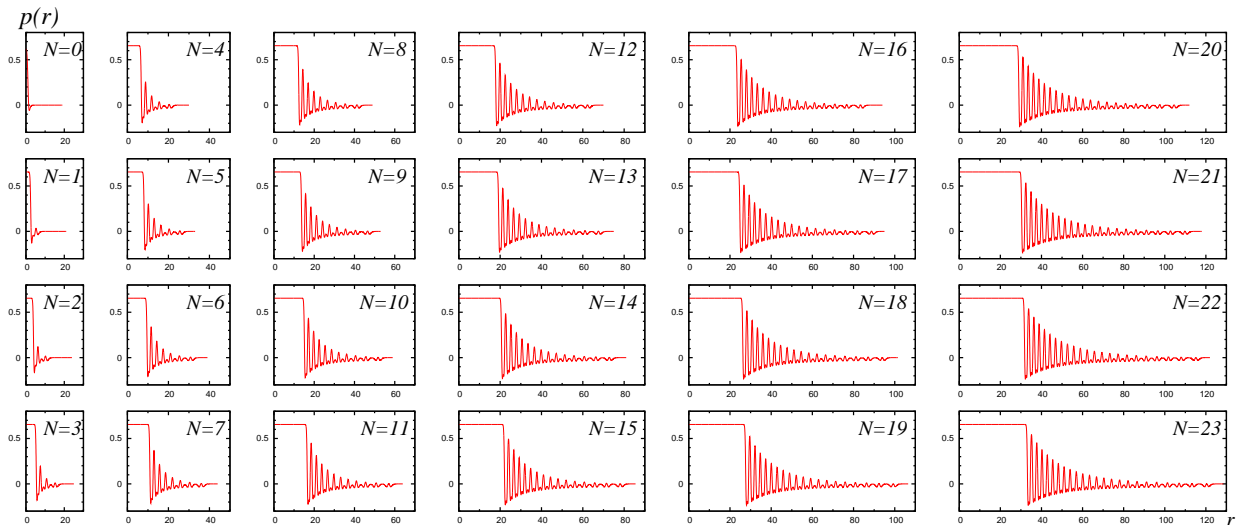


FIG. 6: The pressure distributions $p(r)$ as functions of r for $0 \leq N \leq 23$.

marking the positions of the respective surfaces. For our parameters the system is diffuse, but the “smeared out δ -functions” in $s(r)$ can be seen in Fig. 5 though the “gaps” between the first shells cannot be clearly resolved.

Also this can be understood in the particle picture, where $s(r) \rightarrow 2E_{\text{kin}}(t)$. The zeros of $s(r)$ coincide with the turning points in Fig. 1. The maxima of $s(r)$ occur at the positions where the particle is fastest, which is close to the origin of the particle coordinate¹ in Fig. 1. The characteristic double peaks emerge because the particle is slowed down at the origin by the buckle in U_{eff} . At earlier times (inner region) the friction $F_{\text{fric}} \propto \frac{1}{t}$ is noticeable making the double peaks less symmetric and hard to resolve, see Fig. 5. At later times (outer region) the friction is diminished, and the double peaks are nearly symmetric.

Fig. 6 show that the pressure distribution of the N^{th} excitation changes the sign $(2N + 1)$ times. Although with increasing N the structures are more and more complex, the results are numerically stable and satisfy the stringent tests discussed in App. B. In particular, in all cases the stability condition is satisfied within numerical accuracy, as we will discuss in detail in Sec. V.

Figs. 2–6 demonstrate that with increasing N the system becomes larger and exhibits an increasing degree of complexity. In spite of the complexity, however, the size of the system grows with remarkable regularity, as is shown in Fig. 7. This Figure displays for the excitations $1 \leq N \leq 23$ the respectively first (R_1) and last (R_N) zero of the solutions $\phi(r)$. For $N = 1$ the two radii coincide. We observe that the R_1 and R_N increase linearly with the order of the excitation.

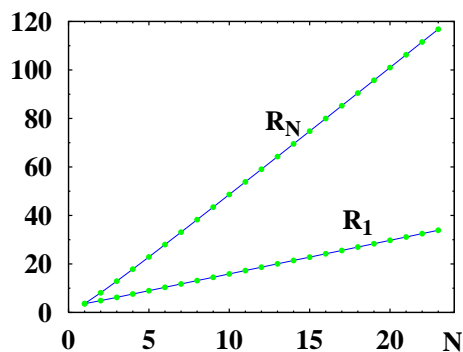


FIG. 7: The positions of the first (R_1) and last (R_N) zero of the N^{th} radial excitation as function of N for $1 \leq N \leq 23$. The discrete data sets are connected by lines to guide the eye.

¹ To recall, the origin in the particle coordinate $x(t)$ corresponds to the zeros of $\phi(r)$. The latter are also the zeros of the charge distribution and close to the minima of $T_{00}(r)$, see above, which emphasizes that all quantities reflect the same shell structure.

IV. GLOBAL PROPERTIES

Above we made three important observations which will allow us to make predictions for the N -behavior of the global (integrated) properties of Q -balls, namely

- (i) the system exhibits a shell structure,
- (ii) the size of the system grows linearly with N ,
- (iii) $\rho_{\text{ch}}(r)$ and $T_{00}(r)$ inside the Q -balls are effectively constant independently of N .

The shell structure of point (i) is evident from Figs. 2–6. The linear growth of point (ii) is apparent from Fig. 7. Point (iii) however requires some explanation. Strictly speaking the fields $\phi(r)$ and consequently $\rho_{\text{ch}}(r)$ and $T_{00}(r)$ are constant only in the inner region, i.e. in about 1/4 of the size of excited Q -balls. However, when integrating we effectively “average” over the oscillatory behavior of these densities in the outer region. Therefore, when speaking about global (integrated) properties we may think in terms of effectively constant densities inside excited Q -balls which motivates assumption (iii).

On the basis of these observations we expect the following N -behavior of the charge Q , mass M , constant d_1 , the surface tension γ , surface energy E_{surf} , and the mean square radii $\langle r_Q^2 \rangle$, $\langle r_E^2 \rangle$, $\langle r_s^2 \rangle$ of respectively the charge, energy, and shear force distributions:

$$Q \propto N^3 \quad (11)$$

$$M \propto N^3 \quad (12)$$

$$d_1 \propto N^8 \quad (13)$$

$$\gamma \propto N \quad (14)$$

$$E_{\text{surf}} \propto N^3 \quad (15)$$

$$\langle r_i^2 \rangle^{1/2} \propto N, \quad i = Q, E, s. \quad (16)$$

The surface energy is given by $E_{\text{surf}} = \int d^3r s(r)$, while $\langle r_Q^2 \rangle = \int d^3r r^2 \rho_{\text{ch}}(r)/Q$ and $\langle r_E^2 \rangle$ is defined analogously. Finally, the mean square radius of the shear forces is $\langle r_s^2 \rangle = \int_0^\infty dr r^2 s(r)/\gamma$ where $\gamma = \int_0^\infty dr s(r)$ denotes the surface tension. Surface energy and surface tension are well motivated notions in the limit $\omega \rightarrow \omega_{\text{min}}$ [23] in which Q -balls behave like liquid drops [21]. But they will also be helpful in our context.

On the basis of the assumptions (ii, iii) we expect the charge Q and mass M to be proportional to the “volume” which grows like N^3 (even though the solutions are too diffuse to make “volume” a well-defined concept). The scaling predictions (16) for the mean square radii also follow straight forwardly from assumption (ii).

The prediction (15) for the surface energy is at first glance counter-intuitive. One would expect E_{surf} to grow with “surface area” $\propto (\text{volume})^{2/3} \propto N^2$. However, we have to take into account the shell structure in point (i). The ground state has one surface, and the N^{th} excitation with its N shells has in addition to that $2N$ surfaces. The contributions of individual surfaces do grow like N^2

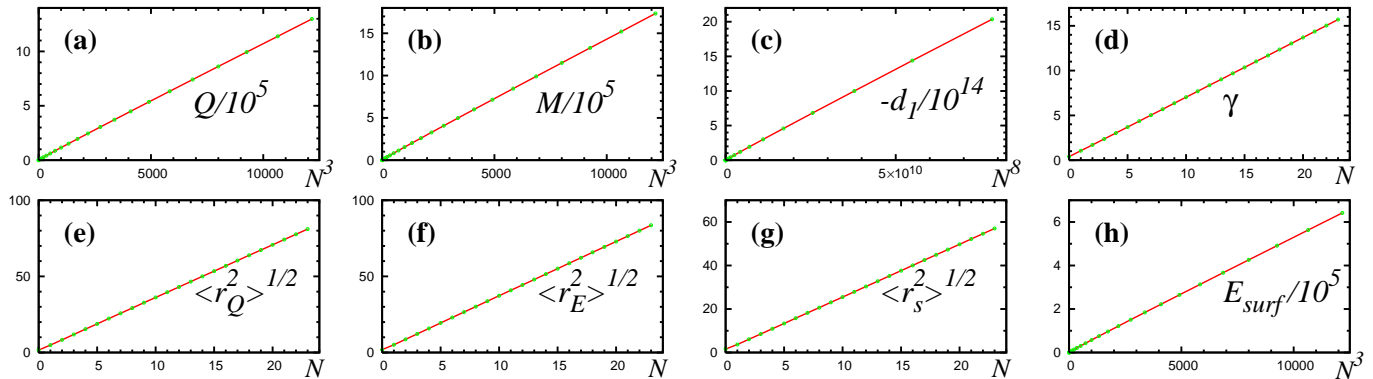


FIG. 8: Various Q -ball properties plotted vs. N^k with the power k chosen according to the predictions in Eqs. (11–16). The shown properties X and the corresponding powers k , written as pairs (X, k) are: (a) charge $(Q, 3)$, (b) mass $(M, 3)$, (c) D -term $(d_1, 3)$, (d) surface tension $(\gamma, 1)$, the square roots of the mean square radii of the (e) charge distribution $(\langle r_Q^2 \rangle^{1/2}, 1)$, (f) energy distribution $(\langle r_E^2 \rangle^{1/2}, 1)$, (g) shear force distribution $(\langle r_s^2 \rangle^{1/2}, 1)$, and (h) the surface energy $(E_{\text{surf}}, 3)$. The discrete data sets are connected by lines to guide the eye.

as the size of the system grows $\propto N$ according to point (i). But also the number of surfaces grows $\propto N$, which yields (15). Similarly, we expect the surface tension γ as defined in [21, 23] to be also proportional to the number of surfaces, hence the prediction (14).

In order to derive the scaling behaviour of d_1 we may use dimensional arguments. The dimensionality of d_1 is $(\text{mass} \times \text{size})^2$ and with mass $\propto N^3$ and size $\propto N$ we obtain the prediction (13). Alternatively we may explore the liquid drop limit in which $d_1^{\text{drop}} = -\frac{4\pi}{3} M \gamma R^4$ where R denotes the radius of the drop [5, 21]. With the scaling predictions (12, 14, 16) for M , γ , and size of the system we are again lead to the prediction (13).

Fig. 8 shows the global properties Q , M , d_1 , γ , $\langle r_i^2 \rangle$ for $i = Q, M, s$ and E_{surf} plotted as functions of N^k with the powers k as predicted in Eqs. (11–16). The results fully confirm the predictions (11–16). Hardly visible in Fig. 8 is that for $N = 0, 1, 2$ the global properties exhibit deviations from the scaling behavior (11–16). But for $N \gtrsim 2$ the numerical results follow Eqs. (11–16) with very good accuracy, see Fig. 8.

In particular, we observe $\gamma \propto N$ as predicted in (14). The more adequate property characterizing the “surface tension” at the “boundary” between Q -matter and vacuum is the rescaled quantity $\gamma_{\text{resc}} = \gamma/(2N + 1)$ which

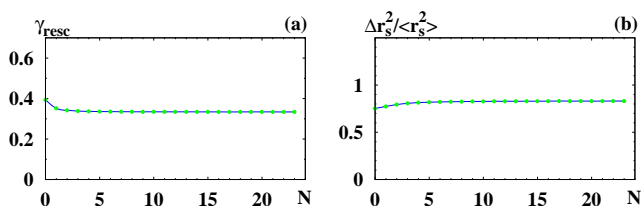


FIG. 9: (a) The true “surface density” $\gamma_{\text{resc}} = \gamma/(2N + 1)$ as function of N . (b) The measure of the diffuseness of the system $\Delta r_s^2 / \langle r_s^2 \rangle$ as function of N .

takes into account that the N^{th} radial excitation has $(2N + 1)$ surfaces. Fig. 9a shows that γ_{resc} is nearly independent of N as expected. We stress that γ_{resc} is an average. Q -matter in excited Q -balls does not possess the same “surface tension” everywhere, otherwise the peaks in $s(r)$ in Fig. 5 would be all equally high.

We would like to stress that although qualitatively here the liquid drop picture is useful, the concept of a surface tension is well justified only in the limit $\omega \rightarrow \omega_{\text{min}}$ where the solutions exhibit “sharp edges” [23]. For ground states $\Delta r_s^2 / \langle r_s^2 \rangle$ can be used as a measure for the diffuseness of the system, where $(\Delta r_s^2)^2 = \langle r_s^4 \rangle - \langle r_s^2 \rangle^2$ with $\langle r_s^4 \rangle = \int_0^\infty dr r^4 s(r) / \gamma$ [21]. If for ground states $\Delta r_s^2 / \langle r_s^2 \rangle \ll 1$ one has “sharp edges” [21]. For our parameters $\Delta r_s^2 / \langle r_s^2 \rangle \simeq 0.75$ for $N = 0$, i.e. this condition is not convincingly realized; the system is diffuse. If we apply this measure also to excitations, we find that they are similarly diffuse to the ground state, see Fig. 9b.

For $\omega \rightarrow \omega_{\text{min}}$ the $s(r)$ would become proportional to the sum of $(2N + 1)$ δ -functions with support at the positions of the surfaces of the shells [21]. If we assume for simplicity the surfaces equidistant and the coefficients of δ -functions equal (this is not accurate, see Sec. III, but will be irrelevant after we take the limit $N \rightarrow \infty$ below) we would expect that $\langle r_s^4 \rangle \propto \sum_{k=1}^{2N+1} k^4 / (2N + 1)$ while $\langle r_s^2 \rangle \propto \sum_{k=1}^{2N+1} k^2 / (2N + 1)$ and

$$\lim_{N \rightarrow \infty} \frac{\Delta r_s^2}{\langle r_s^2 \rangle} = \frac{2}{\sqrt{5}} \quad \text{for } \omega \rightarrow \omega_{\text{min}}. \quad (17)$$

This corresponds numerically to $0.894 \dots$ and is remarkably close to the values observed for $N \gtrsim 2$ in Fig. 9b, even though our ω is not close to ω_{min} . It would be very interesting to test the prediction (17) for ω closer to ω_{min} . But in such situations radial excitations are difficult to find numerically, see App. A.

The shell structure can also be studied by looking at the charge distribution. Since the $\rho_{\text{ch}}(r)$ vanish at the

positions where the fields $\phi(r)$ change sign, this allows one to define exactly where a shell starts and where it ends. The last shell, of course, has no sharp boundary but vanishes exponentially according to (5). Let us describe briefly how the charge is distributed in the largest excitation $N = 23$ our numerical method could handle. The inner region carries about 16.7% of the total charge of this solution, the first shell 1.64%, and the second 1.58% which is a global minimum. From here on the percentages carried by the subsequent shells increase gradually until the last shell contains 8.8% of the total charge.

We did not observe regularities other than with respect to individual shells, but we found an interesting pattern how the charge is partitioned between the inner region, and the shell region. Let us define Q_{inner} as the charge contained between $0 \leq r \leq R_1$ where R_1 denotes the first zero of $\phi(r)$, and let Q_{shells} denote the charge carried by all shells, such that $Q = Q_{\text{inner}} + Q_{\text{shells}}$. The interesting observation is that as N increases $Q_{\text{inner}}/Q \rightarrow \frac{1}{3}$ from above, while $Q_{\text{shells}}/Q \rightarrow \frac{4}{5}$ from below, see Fig. 10a.

Of all global properties studied in this work d_1 shows the strongest variations with N , as it did for ground states when ω was varied [21]. However, when taking the dimensionality of d_1 into account, see above, one finds that the appropriately scaled constant d_1 is bound from above and below. In [21] the following inequality was derived for all solutions of the Q -ball equations of motion

$$0 < -\frac{d_1}{M^2 \langle r_E^2 \rangle} < \frac{5}{9}. \quad (18)$$

In Fig. 10b we see that the radial excitations satisfy the inequality (18).

Finally let us mention the interesting relation of d_1 to the relative “wall width” $\Delta r_s^2 / \langle r_s^2 \rangle$ derived in [21] which can be expressed as

$$-\frac{d_1}{M E_{\text{surf}} \langle r_s^2 \rangle} = \frac{1}{3} \left(1 + \left(\frac{\Delta r_s^2}{\langle r_s^2 \rangle} \right)^2 \right) \xrightarrow{\omega \rightarrow \omega_{\text{min}}} \frac{3}{5}, \quad (19)$$

where in the last step we used (17). Again, although in our calculation ω is not close to ω_{min} we observe in Fig. 10b that the numerical results are close to the limit derived in (19).

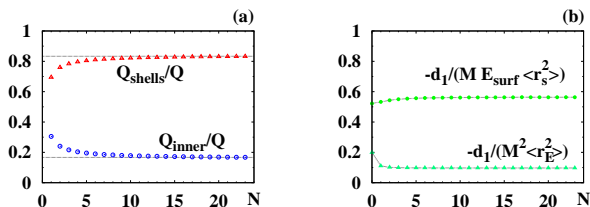


FIG. 10: (a) The relative contributions of the inner region (circles) and the shell region (triangles) to the total charge as function of N . (b) The constant d_1 in units of $M^2 \langle r_E^2 \rangle$ (squares) and $M E_{\text{surf}} \langle r_s^2 \rangle$ (circles) as function of N .

V. STABILITY AND d_1

For all solutions we find $M < m Q$ where $m = \omega_{\text{max}}$ denotes the mass of a Q -quantum. For the ground state this inequality implies absolute stability. But the radial excitations can decay. For all our excitations lighter ground state configurations exist with the same charge.

For example, our first excited state of $\omega^2 = 1.37$ has $Q = 342$ and $M = 461$. The following absolutely stable ground state solutions have the same total charge but a smaller total mass:

- one Q -ball of $\omega^2 = 0.51$ is 1.61 times lighter,
- two Q -balls of $\omega^2 = 0.61$ are 1.45 times lighter,
- three Q -balls of $\omega^2 = 0.68$ are 1.35 times lighter,
- ⋮
- fifteen Q -balls of $\omega^2 = 1.18$ are 1.008 times lighter.

The latter is the threshold for symmetric configurations, and 16 Q -balls with $\omega^2 = 1.21$ would be 0.5% heavier. Also asymmetric configurations with lower energy exist. E.g., the ground states for $\omega^2 = 0.516$ and $\omega^2 = 1.37$ (i.e. the ground state of our excitation) have the same total charge but are 1.55 times lighter than the first excited state of $\omega^2 = 1.37$. The still heavier excitations $N > 1$ have accordingly more decay modes.² In short, all radial excitations are unstable.

Nevertheless, the solutions with $N > 0$ of course also minimize the energy functional, though they correspond to local minima of the action. One way to test this offers the stability condition, or “von Laue-condition” [45],

$$\int_0^\infty dr r^2 p(r) = 0, \quad (20)$$

which was proven to be satisfied for all finite energy solutions in the Q -ball system in [21]. It furthermore was shown that for all finite energy solutions the pressure is positive for small r and negative for large r [21]. In Sec. III we have seen that the pressure distribution of the N^{th} radial excitation exhibits this pattern and changes sign $(2N+1)$ times. It is instructive to look in some more detail how excited Q -balls realize the condition (20).

Fig. 11 shows $r^2 p(r)$ as function of r for the ground state and the radial excitations. In spite of the complexity of the results the condition (20) is satisfied within numerical accuracy which can be quantified as follows. For instance, for the ground state we obtain

² Here we content ourselves to observe that more stable configurations exist, and are not concerned with the dynamics of the possible decays. All numbers quoted for $\omega^2 \neq 1.37$ are from [21].

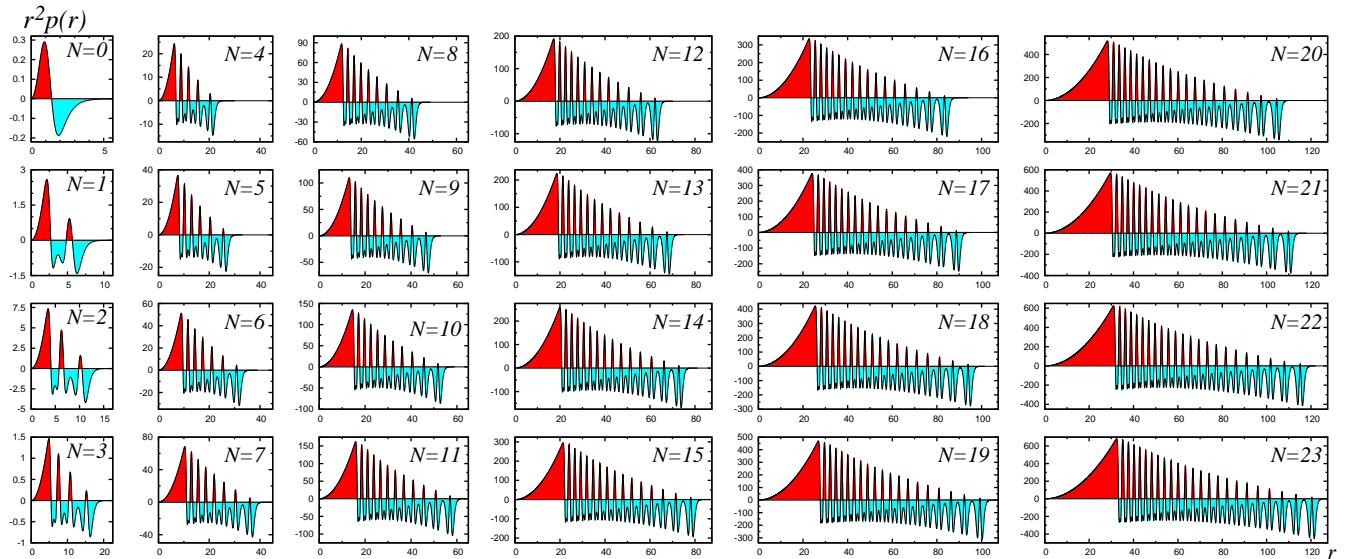


FIG. 11: $r^2 p(r)$ as functions of r for $0 \leq N \leq 23$. Except for the first column the scales on the r -axis are kept constant for a better comparison. The shaded regions above and below the r -axis have equal areas such that $\int_0^\infty dr r^2 p(r) = 0$.

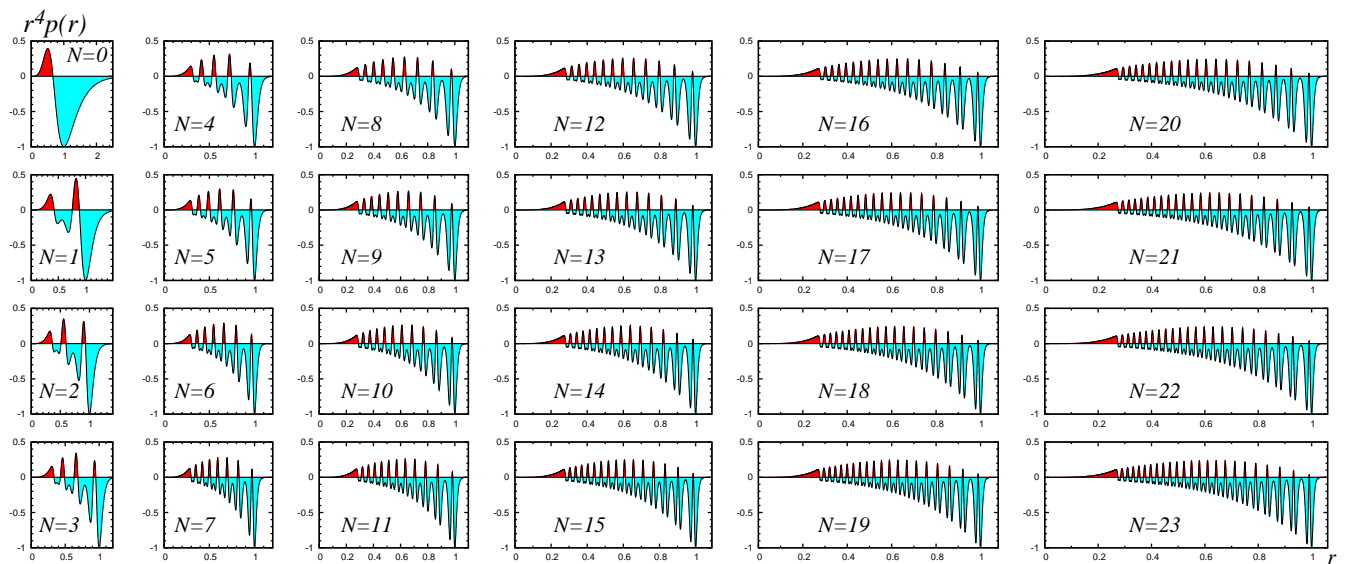


FIG. 12: $r^4 p(r)/C_{\text{last}}$ as functions of r/R_{last} for $0 \leq N \leq 23$, where R_{last} denotes the position of the last minimum of $r^4 p(r)$ and $C_{\text{last}} = |R_{\text{last}}^4 p(R_{\text{last}})|$. With these units the global of all curves occur at $r/R_{\text{last}} = 1$ and assume the value $r^4 p(r)/C_{\text{last}} = -1$ which makes a comparison easier. $r^4 p(r)$ is the integrand of d_1 . The figure demonstrates how the negative sign of d_1 appears.

$|\int_0^\infty dr r^2 p(r)| / \int_0^\infty dr r^2 |p(r)| = \mathcal{O}(10^{-8})$ and similarly up to $N \leq 4$. With increasing N it becomes more difficult to maintain this accuracy. For $N \gtrsim 10$ the accuracy is in the range $\mathcal{O}(10^{-5})$ to $\mathcal{O}(10^{-3})$.

The regions with positive pressure provide forces directed towards outside. These repulsive forces are compensated by negative pressure regions with attractive forces directed towards the center. Repulsive and attractive forces cancel precisely according to (20).

It is interesting to note that the role of the shells is to compensate the repulsive forces from the core. In fact,

on average the shells contribute attractive forces.

In Ref. [21] it was shown that the pattern how the pressure distribution satisfies the condition (20) at once implies that the constant d_1 must have a negative sign. Although the sign of d_1 can also be deduced from the shear forces [21], this indicates a connection between d_1 and stability. In [21] only Q -ball ground states were studied, for which $p(r)$ changes sign only once. Nevertheless the general proof that the stability condition (20) implies $d_1 < 0$ in [21] was formulated assuming that the pressure change the sign an arbitrary odd number of times. This

is the situation we encounter for radial excitations, and our results illustrate how the stability condition (20) determines the sign of d_1 .

Fig. 12 shows $r^4 p(r)$ as functions of r . Clearly, integrating this function over r yields a negative number, and up to a prefactor of $5\pi M$ the constant d_1 , cf. Eq. (10). Our results for the pressure distribution therefore fully confirm the general proof of the negative sign of d_1 from the stability relation (20) formulated in [21].

We remark that in the proof of [21] also the possibility was considered that the $p(r)$ could become zero at some point without changing sign. We do not encounter this situation for the parameters used in this work.

VI. CONCLUSIONS

We presented a study of the energy momentum tensor of Q -balls in a scalar field theory with U(1) symmetry. While in a previous work we investigated in detail ground state solutions for different ω [21], in this work radial excitations of Q -balls were in the focus of our study.

In Ref. [36] the radial excitations $N = 1, 2$ were studied previously for fixed charge Q , in other words the excitations were classified by specifying the charge and order (Q, N) . Here we adopted a different classification scheme and fixed ω , i.e. the excitations are specified by (ω, N) . We were able to find numerically solutions for the ground state $N = 0$ and $1 \leq N \leq 23$ excitations. All solutions obtained in this work were exact solutions of the equations of motion. The numerical results were subject to stringent tests to guarantee their correctness. On the basis of our results reaching high in the spectrum of radial excitations we were able to obtain fascinating insights in the structure of these excitations.

As N grows the systems exhibit increasing degrees of complexity. The radial field of the N^{th} excitation changes the sign N -times. At the positions R_i with $1 \leq i \leq N$ where this happens the otherwise positive charge distribution vanishes exactly, and the energy density shows at positions very close to the R_i clear minima. In other words, the charge is distributed over an inner region with nearly constant density surrounded by N shells, and $T_{00}(r)$ closely follows this pattern. We observed the interesting pattern that, as N increases, the constant density inner region carries 1/6 of the total charge, while the remaining 5/6 are distributed on the shells.

The energy densities show in addition also characteristic spikes at the “edges” of the shells due to the impact of the “surface energy.” The effects of the “surface tension” are reflected with even more clarity in the shear force distributions. We have shown that the system is diffuse for the parameters considered in this work, and discussed in which sense the concepts “surface tension” and “surface energy” are nevertheless useful. The highest degree of complexity is seen in the pressure distributions which change the sign $(2N + 1)$ times.

In spite of the complexity of the solutions, the properties of the excited Q -balls scale with N with great regularity. For instance, the size of the system is proportional to N , independently whether one uses the zeros of the $\phi(r)$ or square roots of various mean square radii to define it. On the basis of general arguments we were able to predict also the scaling of other quantities, for instance $M \propto N^3$ or $d_1 \propto N^8$ which are supported by our numerical results. Remarkably, among all quantities we studied, the D -term varies most strongly with N . Similarly d_1 was the quantity which varied most strongly in the study of ground state solutions as functions of ω [21].

One of the consequences of EMT conservation is the stability (or von-Laue-) condition [5, 45] stating that $\int_0^\infty dr r^2 p(r) = 0$. In [21] this condition was proven analytically to be satisfied for any solution of Q -ball equations of motion, and in this work we could verify numerically that the $p(r)$ of radial excitations with its $(2N + 1)$ precisely integrates to zero with very good numerical precision.

The important result is that the D -term is negative also for all radial excitations. In all approaches where d_1 was studied so far, it was found negative. But only the D -terms of ground states were studied so far, and to best of our knowledge this is the first time excited states are shown to have also negative D -terms.

In [21] a rigorous proof was given that for Q -balls $d_1 < 0$ follows from the stability condition and Q -ball equations of motion. In [21] only ground state solutions were studied for which $p(r)$ changes sign only once. Nevertheless the proof had to be formulated assuming that $p(r)$ could more generally change the sign any odd number of times. The results obtained in this work illustrate that this is not a pathological case which has to be taken into account for the sake of mathematical rigor. Indeed, for excited Q -balls one does encounter such a situation in practice.

In this work we also fully confirm another finding of [21], namely that stability is a sufficient but not necessary condition for d_1 to be negative. In fact, we have shown that all radial excitations obtained in this work are unstable. They correspond to local but not global minima of the action, and can decay into configurations of absolutely stable ground states with the same total charge but a smaller total mass.

The works presented here and in [21] clearly demonstrate the property $d_1 < 0$ for Q -ball systems and, we hope, will inspire rigorous proofs of this property also in other systems. Our results also establish d_1 as a particle property particularly sensitive to variations of parameters of the system. An interesting question remains: can d_1 be ever positive in a physical system?

Acknowledgements. We thank Gerald Dunne and Alex Kovner for helpful discussions. The work was partly supported by DOE contract DE-AC05-06OR23177, under which Jefferson Science Associates, LLC, operates the Jefferson Lab.

Appendix A: Technical details

We assume $\omega > 0$ without loss of generality. Finite energy solutions exist for ω in the range [23]

$$\omega_{\min}^2 \equiv \min_{\phi} \left[\frac{2V(\phi)}{\phi^2} \right] < \omega^2 < \omega_{\max}^2 \equiv V''(\phi) \Big|_{\phi=0}. \quad (\text{A1})$$

For the potential used in this work $0.2 < \omega^2 < 2.2$. The ground states are absolutely stable for $\omega^2 < \omega_{\text{abs}}^2 \approx 1.55$ [21]. For ω close to ω_{\min} it is numerically challenging to handle the ground states, let alone radial excitations. In order to have an absolutely stable ground state, and maximize the chances find numerous radial excitations it is profitable to work close to $\omega_{\text{abs}}^2 \approx 1.55$. In this sense, $\omega = \sqrt{1.37} \approx 0.94 \omega_{\text{abs}}$ is among the ideal choices.

As N increases, see Sec. II, it is necessary to release the particles close to the maximum of U_{eff} given by

$$\phi_{\text{const}}(\omega) = \sqrt{\frac{B}{C} \left(\frac{1}{3} + \frac{1}{6} \sqrt{1 + \frac{6C}{B^2} (\omega^2 - \omega_{\min}^2)} \right)}, \quad (\text{A2})$$

where the subscript reminds that (A2) corresponds to one of the ‘‘stationary’’ solutions $\phi(r) = \text{const}$ of (2) [21], which however do not satisfy the boundary condition for $r \rightarrow \infty$. For our parameters $\phi_{\text{const}} = 1.1045\dots$ and the radial excitations $N \geq 1$ are all within 10^{-6} of this value.

Appendix B: Numerical tests

In view of the complexity of the solutions, it is important to monitor the numerical quality of the solutions.

For that we made the following tests. We checked that

- A. the stability condition (20) is valid,
- B. the equation $\frac{2}{r} s(r) + \frac{2}{3} s'(r) + p'(r) = 0$ is satisfied,
- C. the expressions for d_1 in (10) yield the same result,
- D. $p(0) = 2 \int_0^\infty dr \frac{s(r)}{r}$ is equal to $p(0)$ from (9).

All these relations can be derived from EMT conservation [5, 17] and provide powerful tests for the numerics [21]. We find relative numerical accuracies between $\mathcal{O}(10^{-9})$ and $\mathcal{O}(10^{-3})$ depending on N and the kind of test.

In Sec. V we already reported how the stability condition, test (A), is satisfied numerically. For (B) we checked that $(\frac{2}{r} s(r) + \frac{2}{3} s'(r) + p'(r)) / (\frac{2}{r} |s(r)| + \frac{2}{3} |s'(r)| + |p'(r)|)$ is typically of $\mathcal{O}(10^{-3})$ or smaller, for $r > 0$ and $\forall N$.

Concerning test (C): for instance, for the highest excitation $N = 23$ we were able to handle with our numerics, we obtain from (10): $d_1^p = -2.0366 \times 10^{15}$ using pressure distribution vs. $d_1^s = -2.0360 \times 10^{15}$ from shear forces, which corresponds to a relative accuracy of 3×10^{-4} .

Concerning test (D): we obtain e.g. for $N = 23$ the result $p(0) = 0.654652$ from Eq. (9), while using the above quoted formula yields $p(0) = 0.654655$, which corresponds to a relative accuracy of 5×10^{-5} .

On the basis of these stringent tests we are confident that none of the bumps, peaks, structures in Figs. 2–12 are numerical artifacts, but all details of our numerical solutions reflect the true characteristics of the excited states.

-
- [1] H. R. Pagels, Phys. Rev. **144** (1965) 1250.
 - [2] X. D. Ji, Phys. Rev. Lett. **74**, 1071 (1995).
 - [3] X. D. Ji, Phys. Rev. Lett. **78**, 610 (1997) [arXiv:hep-ph/9603249].
 - [4] M. V. Polyakov and C. Weiss, Phys. Rev. D **60**, 114017 (1999) [arXiv:hep-ph/9902451].
 - [5] M. V. Polyakov, Phys. Lett. B **555** (2003) 57 [arXiv:hep-ph/0210165].
 - [6] J. F. Donoghue and H. Leutwyler, Z. Phys. C **52**, 343 (1991).
 - [7] D. Müller *et al.*, Fortsch. Phys. **42**, 101 (1994). A. V. Radyushkin, Phys. Lett. B **380**, 417 (1996); Phys. Lett. B **385**, 333 (1996); Phys. Rev. D **56**, 5524 (1997). X. D. Ji, Phys. Rev. D **55**, 7114 (1997). J. C. Collins, L. Frankfurt and M. Strikman, Phys. Rev. D **56**, 2982 (1997).
 - [8] X. D. Ji, J. Phys. G **24**, 1181 (1998). A. V. Radyushkin, arXiv:hep-ph/0101225. K. Goeke, M. V. Polyakov and M. Vanderhaeghen, Prog. Part. Nucl. Phys. **47**, 401 (2001). A. V. Belitsky, D. Mueller and A. Kirchner, Nucl. Phys. B **629**, 323 (2002) [arXiv:hep-ph/0112108]. M. Diehl, Phys. Rept. **388** (2003) 41. A. V. Belitsky and A. V. Radyushkin, Phys. Rept. **418**, 1 (2005).
 - [9] C. Adloff *et al.* [H1 Collaboration], Phys. Lett. B **517**, 47 (2001). A. Aktas *et al.*, Eur. Phys. J. C **44**, 1 (2005) F. D. Aaron *et al.*, Phys. Lett. B **659**, 796 (2008); Phys. Lett. B **681**, 391 (2009). S. Chekanov *et al.* [ZEUS Collaboration], Phys. Lett. B **573** (2003) 46; JHEP **0905**, 108 (2009).
 - [10] A. Airapetian *et al.* [HERMES Collaboration], Phys. Rev. Lett. **87**, 182001 (2001); Phys. Rev. D **75**, 011103 (2007); JHEP **0806**, 066 (2008); JHEP **0911**, 083 (2009); Nucl. Phys. B **829**, 1 (2010); Nucl. Phys. B **842**, 265 (2011). F. Ellinghaus [HERMES Collaboration], Nucl. Phys. A **711**, 171 (2002) [hep-ex/0207029].
 - [11] S. Stepanyan *et al.* [CLAS Collaboration], Phys. Rev. Lett. **87**, 182002 (2001). S. Chen *et al.*, Phys. Rev. Lett. **97**, 072002 (2006). F. X. Girod *et al.*, Phys. Rev. Lett. **100**, 162002 (2008). G. Gavalian *et al.*, Phys. Rev. C **80**, 035206 (2009).
 - [12] C. Munoz Camacho *et al.* [Jefferson Lab Hall A Collaboration], Phys. Rev. Lett. **97**, 262002 (2006). M. Mazouz *et al.*, Phys. Rev. Lett. **99**, 242501 (2007).
 - [13] N. Mathur, S. J. Dong, K. F. Liu, L. Mankiewicz and

- N. C. Mukhopadhyay, Phys. Rev. D **62**, 114504 (2000)
P. Hägler *et al.* [LHPC collaboration], Phys. Rev. D **68**, 034505 (2003); Phys. Rev. D **77**, 094502 (2008).
J. D. Bratt *et al.*, Phys. Rev. D **82**, 094502 (2010).
M. Göckeler *et al.* [QCDSF Collaboration], Phys. Rev. Lett. **92**, 042002 (2004)
- [14] B. Kubis and U. G. Meissner, Nucl. Phys. A **671**, 332 (2000) [Erratum-ibid. A **692**, 647 (2001)]. J. W. Chen and X. D. Ji, Phys. Rev. Lett. **88**, 052003 (2002).
A. V. Belitsky and X. D. Ji, Phys. Lett. B **538**, 289 (2002). S.-I. Ando, J.-W. Chen and C.-W. Kao, Phys. Rev. D **74**, 094013 (2006). M. Diehl, A. Manashov and A. Schäfer, Eur. Phys. J. A **29**, 315 (2006).
- [15] E. Megias, E. Ruiz Arriola, L. L. Salcedo and W. Broniowski, Phys. Rev. D **70**, 034031 (2004) E. Megias, E. Ruiz Arriola and L. L. Salcedo, Phys. Rev. D **72**, 014001 (2005) W. Broniowski and E. R. Arriola, Phys. Rev. D **78**, 094011 (2008)
- [16] V. Y. Petrov *et al.*, Phys. Rev. D **57**, 4325 (1998).
P. Schweitzer *et al.*, Phys. Rev. D **66**, 114004 (2002).
J. Ossmann *et al.*, Phys. Rev. D **71**, 034011 (2005).
M. Wakamatsu, Phys. Lett. B **648**, 181 (2007).
- [17] K. Goetze *et al.*, Phys. Rev. D **75**, 094021 (2007); Phys. Rev. C **75**, 055207 (2007).
- [18] C. Cebulla *et al.*, Nucl. Phys. A **794**, 87 (2007).
H.-Ch. Kim, P. Schweitzer and U. Yakhshiev, arXiv:1205.5228 [hep-ph].
- [19] S. Liuti and S. K. Taneja, Phys. Rev. C **72**, 032201 (2005). V. Guzey and M. Siddikov, J. Phys. G **32** (2006) 251
- [20] E. Witten, Nucl. Phys. B **160**, 57 (1979), and Nucl. Phys. B **223**, 433 (1983).
- [21] M. Mai and P. Schweitzer, arXiv:1206.2632 [hep-ph].
- [22] R. Friedberg, T. D. Lee and A. Sirlin, Phys. Rev. D **13**, 2739 (1976).
- [23] S. R. Coleman, Nucl. Phys. B **262**, 263 (1985) [Erratum-ibid. B **269**, 744 (1986)].
- [24] A. M. Safian, S. R. Coleman and M. Axenides, Nucl. Phys. B **297**, 498 (1988).
- [25] A. G. Cohen, S. R. Coleman, H. Georgi and A. Manohar, Nucl. Phys. B **272**, 301 (1986).
- [26] M. G. Alford, Nucl. Phys. B **298**, 323 (1988).
- [27] T. D. Lee and Y. Pang, Phys. Rept. **221**, 251 (1992).
- [28] A. Kusenko, Phys. Lett. B **404**, 285 (1997); Phys. Lett. B **405**, 108 (1997). A. Kusenko and M. E. Shaposhnikov, Phys. Lett. B **418**, 46 (1998).
- [29] S. Kasuya and M. Kawasaki, Phys. Rev. D **61**, 041301 (2000).
- [30] T. Multamaki and I. Vilja, Nucl. Phys. B **574**, 130 (2000). F. Paccetti Correia and M. G. Schmidt, Eur. Phys. J. C **21**, 181 (2001). T. A. Ioannidou, A. Kouiroukidis and N. D. Vlachos, J. Math. Phys. **46**, 042306 (2005).
- [31] N. Graham, Phys. Lett. B **513**, 112 (2001).
- [32] S. S. Clark, Nucl. Phys. B **756**, 38 (2006). M. Fairbairn, A. C. Kraan, D. A. Milstead, T. Sjostrand, P. Skands and T. Sloan, Phys. Rept. **438**, 1 (2007).
- [33] D. P. Clougherty, Phys. Rev. Lett. **96**, 045703 (2006).
- [34] M. Schmid and M. Shaposhnikov, Nucl. Phys. B **775**, 365 (2007).
- [35] Y. Verbin, Phys. Rev. D **76**, 085018 (2007). B. Hartmann and J. Riedel, arXiv:1204.6239 [hep-th].
- [36] M. S. Volkov and E. Wahnert, Phys. Rev. D **66**, 085003 (2002).
- [37] M. Gleiser and J. Thorarinson, Phys. Rev. D **73**, 065008 (2006).
- [38] V. A. Gani, N. B. Konyukhova, S. V. Kurochkin, and V. A. Lensky, USSR Comput. Math. Math. Phys. **44**, 1968 (2007).
- [39] N. Sakai and M. Sasaki, Prog. Theor. Phys. **119**, 929 (2008). T. Tamaki and N. Sakai, Phys. Rev. D **81**, 124041 (2010). N. Sakai, H. Ishihara and K.-I. Nakao, Phys. Rev. D **84**, 105022 (2011)
- [40] M. I. Tsumagari, E. J. Copeland and P. M. Saffin, Phys. Rev. D **78**, 065021 (2008). E. J. Copeland and M. I. Tsumagari, Phys. Rev. D **80**, 025016 (2009).
- [41] P. Bowcock, D. Foster and P. Sutcliffe, J. Phys. A **42**, 085403 (2009).
- [42] H. Arodz and J. Lis, Phys. Rev. D **77**, 107702 (2008); Phys. Rev. D **79**, 045002 (2009).
- [43] G. Gabadadze and R. A. Rosen, Phys. Lett. B **666**, 277 (2008).
- [44] L. Campanelli and M. Ruggieri, Phys. Rev. D **80**, 036006 (2009).
- [45] M. von Laue, Ann. Phys. (Leipzig) **340**, 524 (1911).
I. Białynicki-Birula, Phys. Lett. A **182**, 346 (1993)